Photodiagnosis and Photodynamic Therapy 27 (2019) 317–326

Contents lists available at ScienceDirect

Photodiagnosis and Photodynamic Therapy

journal homepage: www.elsevier.com/locate/pdpdt

Photothermal versus photodynamic treatment for the inactivation of the bacteria *Escherichia coli* and *Bacillus cereus*: An *in vitro* study

Heba ElSayed ElZorkany[a,b,*], Tareq Youssef[b], Mona B Mohamed[b], Rehab M Amin[b]

[a] Nanotechnology and Advanced Materials Central Lab, Agriculture Research Center, El Gamaa St., Giza, Egypt
[b] National Institute of Laser Enhanced Sciences, Cairo University, Giza, Egypt

ARTICLE INFO

Keywords:
Photoactivated disinfection (PAD)
Antibacterial
Low power laser light
Photo-toxicity
Multidrug-resistance (MDR)
Antimicrobial photodynamic therapy

ABSTRACT

The widespread occurrence of microbial pathogens, including multidrug-resistant (MDR) bacteria, has ignited research efforts to discover alternative strategies to combat infections in patients. Recently, photodynamic therapy (PDT) and photothermal therapy (PTT) have been proposed for the inactivation of pathogens. Although PDT and PTT are very promising antipathogenic tools, further effort is needed to determine their real impact on pathogens apart from the effects of individual elements involved in the photodynamic/photothermal processes, *i.e.*, light, photosensitizers (PSs), and nanoparticles. Accordingly, in the current study, toluidine blue O (TBO) and gold nanoparticles (GNP) were used as generators of reactive oxygen species (ROS) and hyperthermia in the presence of light, respectively. *Escherichia coli (E. coli)* and *Bacillus cereus (B. cereus*) bacteria were chosen as examples of gram-negative and gram-positive bacteria, respectively. Before the bactericidal activity of PDT was assessed, the aggregation of TBO and its effect on the growth of both strains of bacteria were studied. Additionally, *E. coli* and *B. cereus* were exposed to a range of doses of 633 nm helium-neon laser light to investigate its effect. In a separate set of experiments, the bactericidal activity of PTT was assessed after the effects of GNP and green light (530 nm) had been assessed. The results showed that PDT and PTT should be considered useful tools for bacterial eradication even when the light, PSs, and nanoparticles are each used at doses safe for bacterial growth. Moreover, different photodynamic responses were observed for *E. coli* and *B. cereus*, and light from a 633 nm laser and a 530 nm light-emitting diode (LED) showed disparate responses when applied alone to both bacteria.

1. Introduction

According to recent studies, antimicrobial agent misuse has become a problematic issue worldwide [1]. For example, in Egypt, misused antibiotics compose almost a third of all prescribed antibiotics [2–4]. Ultimately, this causes serious consequences, such as the prevalence of antimicrobial resistance genes among certain pathogens in Egyptian hospitals [5]. Therefore, developing new effective alternatives to traditional antibiotics has become an urgent need because of the multidrug-resistant (MDR) strains of some pathogenic bacteria, especially gram-negative bacteria such as *E. coli, Klebsiella pneumoniae, Pseudomonas aeruginosa* and *Acinetobacter* spp., which have developed resistance to most or all available antibiotics [6].

Fortunately, new therapies have emerged, representing an auspicious alternative way to fight pathogenic bacteria. Photodynamic therapy (PDT) and photothermal therapy (PTT) are some of those promising alternatives. The basis of implementing cell destruction by PDT is the *in situ* generation of reactive oxygen species (ROS), such as singlet oxygen and free radicals, when the photosensitizing agent is exposed to light with the appropriate wavelength [7–9]. These products cause disarrangements in the cell wall and DNA that induce irreversible damage. PDT involves both photophysical and photochemical steps and has several therapeutic applications, such as in treatments against oral and skin infections [8,10,11]. Due to the high affinity of certain photosensitizers (PSs) to bacterial membranes, the short half-life and the short diffusion paths of ROS, strong and local disinfection can be achieved. Moreover, the nonspecific mechanism of action of PDT renders the development of bacterial resistance unlikely [12].

The phenothiazinium class of multifactorial photosensitizing agents has extensive usage in pharmacology and biomedicine. Phenothiazine derivatives are truly broad-spectrum since they are active against bacteria, fungi, viruses, and protozoa, again at variance with the targeting of conventional, single-class antimicrobials [13]. The phenothiazinium derivative toluidine blue O (TBO) is a cationic membrane-active

* Corresponding author at: Nanotechnology and Advanced Materials Central Lab, Agriculture Research Center, Giza, Egypt.
E-mail address: heba.elzorkany@namcl.sci.eg (H.E. ElZorkany).

https://doi.org/10.1016/j.pdpdt.2019.06.020
Received 17 April 2019; Received in revised form 18 June 2019; Accepted 24 June 2019
Available online 25 June 2019

metachromatic dye [14,15] with high affinity for acidic tissue components [16]. TBO shows great clinical potential as a photoantimicrobial agent, particularly against oral pathogens [17]. However, it has a wide range of antipathogenic activities [18].

In addition, the rapid growth of nanotechnology has provided many types of materials for biomedical applications, including use in the fields of antimicrobials, imaging and therapeutics, and persistent biofouling [19]. The generation of photothermally sensitized agents (PTSs), such as gold nanoparticles (GNP), has led to plasmonic photothermal therapy (PPTT) [20]. According to Pissuwan et al, there are two properties of gold that are most relevant: resistance to oxidation and plasmon resonance with light. The surface plasmon resonance (SPR) for ordinary gold nanospheres occurs at ˜520 nm (corresponding to green light) [21]. Under the irradiation of light with the appropriate wavelength, GNP generate moderate heat *in situ*, which is termed hyperthermia. Hyperthermia leads to irreversible cell damage by causing protein denaturation and coagulation, cell membrane destruction, and bubble formation around GNP upon irradiation [22,23]. Although there is a great interest in using rod-shaped GNP for PTT due to their great ability to generate hyperthermia upon exposure to visible and near-IR radiation, sphere-shaped GNP also act as a suitable antimicrobial tool. They are easier to prepare and manipulate, possess hardly any cytotoxicity in the dark, and can generate sufficient hyperthermia upon exposure to green light [24].

Both PDT and PTT have the advantage of triple selectivity: (1) the PS/PTS can be targeted to its destination cell or tissue, (2) non-irradiated PSs/PTSs have pharmacodynamic inertia, and (3) the illumination can be spatially confined to a lesion [25,26]. Moreover, prior studies have demonstrated that PDT/PTT reduced the viability and biofilm formation of strongly resistant bacteria to approximately 30%, and the latter was reduced even further when bacteria pre-exposed to PDT were treated with antibiotics such as gentamicin [27].

Herein, we are attempting to demonstrate an alternative to conventional antimicrobial drugs. The present work aims to demonstrate the antimicrobial activity of two new promising therapies, PDT and PTT, on both gram-negative (G-ve) and gram-positive (G + ve) bacteria using TBO and GNP as representative PSs and photothermal sensitizers, respectively.

2. Materials and methods

2.1. Bacteria

E. coli, as a representative G-ve bacteria, and *B. cereus*, as a representative G + ve bacteria, were isolated, purified, identified, and kindly provided by Prof. Jehan Al Moghazy, Food Safety and Biotechnology Laboratory, Regional Center for Food and Feed, Agriculture Research Center, Egypt. *E. coli*was grown overnight aerobically on Luria agar (LA, Difco, France) at 37 °C. *B. cereus* was grown aerobically on nutrient agar (LAB M, UK) at 37 °C. A single colony of each type of bacteria was isolated from an agar plate and inoculated in Luria broth (LB) medium. The optical density (OD) of each bacterial suspension at 700 nm was adjusted to 0.04 using a double-beam UV–vis spectrophotometer (T80 + , PG Instruments, UK), which is approximately equal to 9×10^3 cells/ml for *E. coli* and 7×10^3 cells/ml for *B. cereus*.

2.2. Photodynamic therapy (PDT)

2.2.1. Aggregation study of toluidine blue O (TBO)

The aggregation of TBO molecules is a problematic issue that may conflict with its potential for PDT [28]. This is because the photosensitization process relies on an initial efficient interaction of incident light with the PS molecules. To study the optical properties of TBO and its aggregation, TBO powder (SERVA Electrophoresis, USA) was dissolved in water and used without further purification. UV–vis absorption spectra of eight different concentrations of TBO ranging from 0.1 to 1000 μM were acquired between 400 and 800 nm. Furthermore, fluorescence emission spectra of the same concentrations of TBO were obtained using a spectrofluorometer (PerkinElmer LS 55, USA). Samples were excited at 633 nm, and the emission band was monitored in the range of 650–750 nm. The excitation and emission slit widths were set at 10 nm. All measurements were performed in Milli-Q water at room temperature and neutral pH.

2.2.2. PDT parameters

For the PDT experiment, 150 μl of each bacterial suspension was seeded in each well of a 96-well microtiter plate with a flat bottom. A He-Ne laser (632.8 nm, 10 mW, Carlsbad, California 92,008) was used as a source of irradiation with a beam spot diameter of 1 mm that had been spread by using a concave lens until reaching 2.5 cm.

Each treatment was tested in triplicate. At the end of a treatment, 20 μl was pipetted out of each well, serially diluted and plated on LB agar. Then, Petri dishes were incubated in an aerophilic atmosphere for 18 h at 37 °C. The number of colony-forming units (CFU) was counted, and cell survival relative to that of the control was calculated for each group of treated samples according to equation (2.1) [29]:

$$\% \text{ survival relative to control} = \text{CFU}_{\text{treated}}/\text{CFU}_{\text{Control}} \quad (2.1)$$

2.2.3. Assessment of the photodynamic effect of TBO on bacterial growth

Before the photodynamic effect of TBO on *E. coli* and *B. cereus* was studied, it was necessary to observe the effect of each element participating in the PDT process independently. Thus, experiments with each bacterial strain were divided into four groups: (1) *E. coli* and *B. cereus* were incubated with different concentrations of TBO in dark conditions (L-P +); (2) both strains of bacteria were exposed to six different doses of He-Ne laser light, ranging from 0.122 to 2.44 J/cm^2, without TBO (L + P-); (3) both strains of bacteria were pre-incubated with different concentrations of TBO (10–90 μM) in a 96-well microtiter plate at 37 °C for 20 min, followed by irradiation with the He-Ne laser for 20 min (L + P +); and (4) bacterial cells were exposed to neither the PS nor the laser (control, L-P-).

The PDT experiments were performed in 96-well plates as previously mentioned (Section 2.3). CFU were counted, and the cell survival relative to that of the control was calculated.

2.2.4. TBO release upon He-Ne irradiation

To assess the release of TBO molecules from *E. coli* cells upon He-Ne irradiation [30], *E. coli* cells were spun down and resuspended in phosphate-buffered saline (PBS) at 9×10^3 cells/ml. The suspension was divided into four aliquots; each aliquot was incubated with TBO for 20 min at 37 °C. The final TBO concentrations were 1, 10, 30 and 50 μM. Subsequently, the TBO-bacteria suspensions were exposed to a He-Ne laser and then filtered using a 0.20 μm syringe filter (CHMLAB, USA). The absorption of the filtrate was measured at 633 nm to estimate the change in TBO concentration in the filtrate. The previous step was repeated for each irradiation dose (1.35, 4, and 6.75 J/cm^2).

2.3. Photothermal therapy (PTT)

2.3.1. Preparation of gold nanoparticles (GNP)

GNP were prepared by the chemical reduction of gold ions in aqueous solution. [31,32] In brief, 5 ml of 1 mM gold (III) chloride trihydrate (Sigma-Aldrich, USA) was added to 40 ml of boiling 1% sodium

citrate dihydrate (Sigma-Aldrich, USA) containing 0.5 g of polyvinyl pyrrolidone or polyvinyl alcohol (PVP or PVA, respectively, Sigma-Aldrich, USA) as a capping agent. The colour of the solution changed from pale yellow to deep red, indicating the formation of GNP. The PVP/PVA polymer arrested the newly formed nanoparticles to prevent aggregation and further growth of the particles. All glassware was prewashed by aqua regia. The preparation was performed in Milli-Q water. The prepared nanoparticles were then characterized using UV–vis absorption spectroscopy, transmission electron microscopy (TEM) and dynamic light scattering (DLS).

2.3.2. GNP characterization

UV-Vis spectra of a diluted solution of the prepared GNP were recorded within the range of 400–800 nm in aqueous medium. Additionally, the size distribution of the particles in the sample and the polydispersity index (PDI) were estimated using a Zetasizer Nano-ZS (Malvern Instruments Ltd, UK).

Furthermore, the morphology of the prepared GNP and their particle size were examined using a TEM (JEOL 2010 F, Japan) gun operating at an accelerating voltage of 120 kV. A drop from a dilute sample solution was deposited on an amorphous carbon-coated copper grid and left to dry at room temperature, forming a monolayer.

2.3.3. PTT parameters

For the PTT experiment, 150 µl of each bacterial suspension was seeded in each well of a 96-well microtiter plate with a flat bottom. An LED (530 nm, 85 mW, Photon Co., Egypt) was used as a source of irradiation, with a beam spot diameter of 6 cm.

Each treatment was tested in triplicate. At the end of each treatment, 20 µl were pipetted from each well and spread on an LB agar plate. Plates were incubated in a microaerophilic atmosphere for 18 h at 37 °C. The numbers of CFU were counted, and the cell survival relative to that of the control was calculated for each group of treated samples according to Eq. (2.1).

2.3.4. Assessment of the photothermal effect on bacterial growth

To study the photothermal effect of GNP on *E. coli* and *B. cereus,* each bacterial suspension was divided into four groups. (1) Bacterial cells were pre-incubated with different concentrations of GNP-PVP/GNP-PVA (10, 20 and 30 µM) in dark conditions (L-G+). (2) Bacterial cells were exposed to three different doses of LED light, 0.9, 2.7 and 3.6 J/cm^2, in a 96-well microtiter plate without GNP (L + G-). (3) Bacterial cells were incubated with GNP for 20 min, followed by irradiation with LED for 5 min (L + G+). (4) Bacterial cells were not exposed to either the GNP or LED (L-G-). The bacterial growth of each group was estimated relative to that of the control group (L-G-).

2.4. Estimation of live/dead bacteria by confocal fluorescent microscopy

To examine the membrane integrity, control and PDT- and PTT-treated cells were washed 3× with PBS, and the pellet was resuspended in 100 µl of PBS containing 10 µl of a 1:1 mixture of propidium iodide (PI) and acridine orange (AO) stains. After incubating the cells with PI/AO mixture for 30 min in the dark, 10 µl of each sample was placed on a coverslip and examined with a 63x confocal laser microscope (CLSM, LSM 710, Carl Zeiss, Germany). While AO stains the live cells and exhibits green fluorescence, PI enters through the membranes of only dead cells and exhibits red fluorescence [33].

2.5. Statistical analysis

All experiments were performed in triplicate. Cell survival is expressed as the mean ± standard error (SE), and the significance was calculated by Student's ANOVA test using GraphPad Prism 7.00, where values of $p < 0.05$ were considered statistically significant. Graphs are marked as follows: * significant at $p < 0.05$, ** significant at $p < 0.01$, *** significant at $p < 0.001$, and **** significant at $p < 0.0001$ according to Student's ANOVA test.

3. Results

3.1. PDT

3.1.1. Spectroscopic characterization of toluidine blue O (TBO)

Fig. 1A shows the UV–vis spectral analysis of TBO (50 µM), whose absorption spectrum possesses a distinct peak at 633 nm. Additionally, there is a shoulder at 590 nm due to the presence of dimers, which occurs at even very low concentrations. [34] Fig. 1B shows the fluorescence emission of TBO at the same concentration; it has a maximum emission at 664 nm when excited at 633 nm.

Fig. 2 illustrates the TBO aggregation as revealed by UV–vis absorption spectroscopy. Absorbance increased consistently as the concentration increased from 0.1 to 1000 µM, but at higher TBO concentrations, the absorbance peak split into two peaks. The first peak has a maximum absorbance at 590 nm (λ_{590}), and the second peak has a maximum absorbance at 633 nm (λ_{633}). The ratio of the OD at λ_{590} to the OD at λ_{633} increased with increasing concentration. At a concentration of 100 µM, the OD at λ_{590} was higher than that at λ_{633} due to the particle aggregates, which were mostly dimers. Furthermore, at the concentration of 1000 µM, the absorption band became very broadened with a plateau shape at the spectral maximum, which indicates the formation of a higher-order aggregate species.

Fig. 3 shows the emission spectra of different concentrations of TBO (0.1–1000 µM). The emission behaviour was analogous to the absorption behaviour: the emission increased with increasing concentration

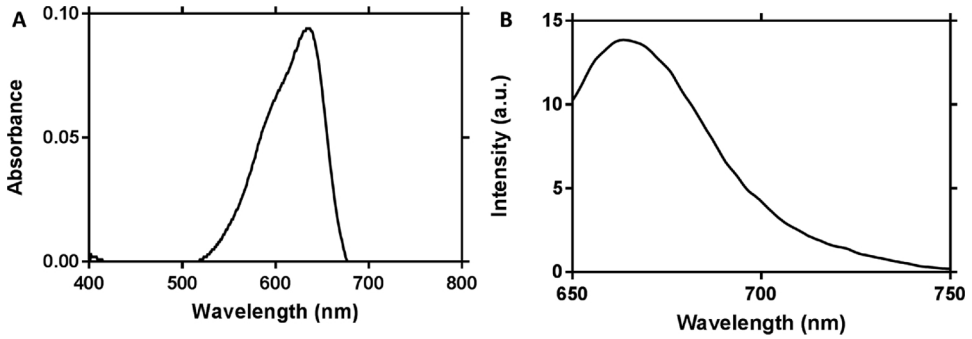

Fig. 1. Spectrum of 50 µM TBO in water: A and B graphs illustrate UV–vis absorption (normalized) and fluorescence emission, respectively.

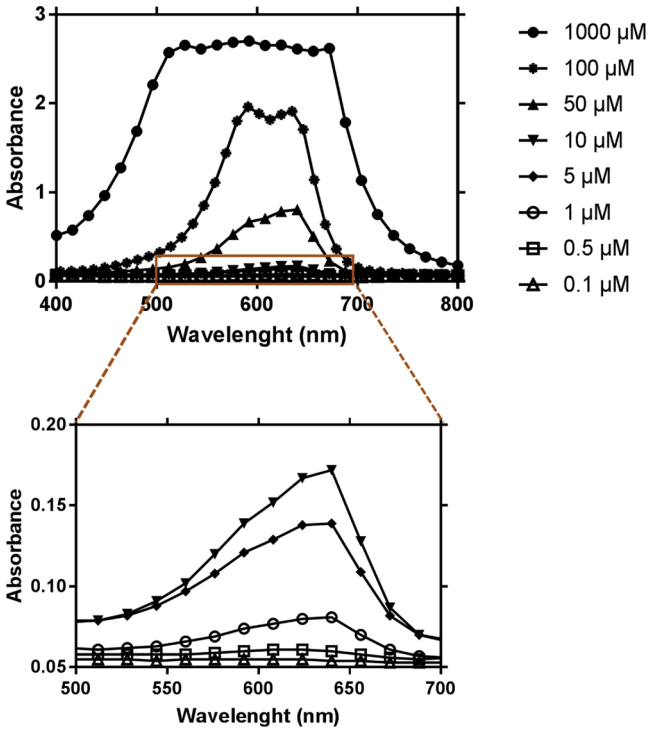

Fig. 2. UV–vis absorption spectra of aqueous TBO solutions of different concentrations.

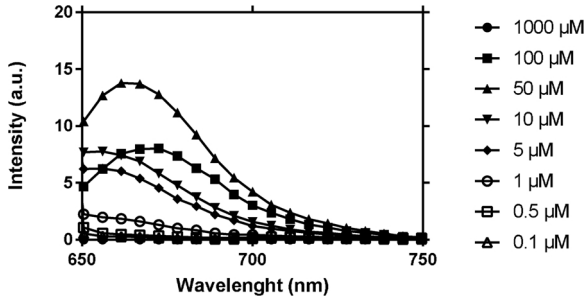

Fig. 3. Fluorescence emission spectra of different concentrations of aqueous TBO solutions.

up to 50 µM, but then decreased; at 1000 µM, the emission was almost zero.

3.1.2. Photodynamic toxicity of TBO

Fig. 4A shows that when *E. coli* and *B. cereus* were incubated with TBO without irradiation (L-P+), each strain showed approximately 100% survival relative to that of the control group (L-P-) up to a TBO concentration of 90 µM. Up to a concentration of 90 µM, TBO did not affect either bacterial strain in dark conditions.

To study the phototoxicity caused by the He-Ne laser alone, six different irradiation doses ranging from 0.122 up to 2.44 J/cm^2 were applied to *E. coli* and *B. cereus* cells in the absence of PSs (L + P-).

The results (Fig. 4B) revealed that a significant effect occurred. At a low dose of the He-Ne laser, an enhancement effect was observed for both bacterial strains. This proliferation effect reached its maximum at 0.6 J/cm^2, where a 165% increase in *E. coli* cell survival and more than a 176% increase in *B. cereus* cell survival were observed.

Further increasing the irradiation dose causes the enhancement effect of the He-Ne laser on bacterial cells to decrease. This decrease in the enhancement started from an energy dose of 1.8 J/cm^2 for both bacterial strains, but it was more evident for *B. cereus* than for *E. coli*. At a dose of 2.4 J/cm^2, the difference in survival relative to the control survival was nonsignificant in both types of bacteria.

Next, the PDT effect on *E. coli* and *B. cereus* (L + P+) was assessed by incubating the bacterial suspensions with different concentrations of TBO and then irradiating them with 2.4 J/cm^2 from the He-Ne laser. Fig. 4C shows that TBO had a significant inhibitory effect on the survival of treated bacteria relative to that of the control after treatment with the He-Ne laser. This inhibition increased with increasing TBO concentration for a fixed dose of laser light. Ninety percent of colonies were depleted after treatment with 90 µM TBO (Fig. 5).

3.1.3. TBO release from E. Coli upon He-Ne irradiation

To investigate membrane destruction and consequent TBO release from *E. coli,* the TBO-*E. coli* suspension filtrate was collected immediately after the PDT experiment, and the UV–vis absorption at 633 nm was examined. Fig. 5 shows an increase in absorption at 633 nm with increasing irradiation time, which indicates an increase in the amount of TBO in the surrounding medium.

3.2. Effect of PTT on bacterial growth

To study the efficiency of PTT as an antibacterial treatment, spherical GNP were prepared by the citrate reduction method using PVP or PVA as a capping agent. Then, different characterization techniques were applied to investigate the absorption, size, and shape of the prepared GNP-PVP/GNP-PVA.

3.2.1. Characterization of gold nanoparticles (GNP)

The UV–vis absorption spectrum of the prepared GNP-PVP showed an absorption maximum at 519 nm, as shown in the lower panel of Fig. 6(A). The TEM micrographs of GNP-PVP inset in the same figure confirm the formation of spherical particles with an average size of 15 ± 3 nm. According to DLS, the size distribution of the sample exhibits a peak at approximately 35 nm (Fig. 6(B)). The PDI values of the sample were typically 0.5.

The UV–vis absorption, TEM, and DLS data of the prepared GNP-PVA are in the supplementary materials (Fig. 1S).

3.2.2. PTT effect of GNP on bacterial growth

When incubating *E. coli* and *B. cereus* cells with GNP in dark conditions (L-G+), we observed different responses for the two strains (Fig. 7(A)). *E. coli* incubated with up to 50 µM GNP-PVP exhibited normal growth relative to that of the control group (L-G-), but increasing the GNP-PVP concentration from 50 to 110 µM enhanced cell growth to more than 100% that of the control. On the other hand, *B. cereus* cells incubated with GNP-PVP in the dark showed normal growth relative to that of the control at all concentrations up to 110 µM. The results illustrated in the supplementary materials (Fig. 2S) showed that incubating *E. coli* and *B. cereus* cells with GNP-PVA in the dark resulted in the number of surviving bacteria decreasing relative to that of the control groups. On the basis of these results, GNP-PVP was chosen for the PTT experiment, while GNP-PVA was excluded due to its toxicity in the dark.

Fig. 7B shows the effect of green LED light alone on *E. coli* and *B. cereus* cells (L + G). Irradiation with LED light of up to 3.6 J/cm^2 had no significant effect on *E. coli* cells. However, green light reduced the growth of *B. cereus* to 90%, 72% and 55% relative to that of the control at irradiation of 0.9, 2.7 and 3.6 J/cm^2, respectively.

The combination of GNP and LED led to a significant reduction in bacterial survival relative to that of the control. Combining the right light dose and suitable concentrations of GNP-PVP resulted in 40% inhibition of *E. coli* survival and approximately 75% inhibition of *B. cereus* survival relative to the survival of the control groups (Fig. 7C).

Fig. 8 illustrates confocal imaging of *E. coli* and *B. cereus* stained with a mixture of AO/PI. The control samples for both strains show almost entirely green coloured cells. In contrast, PDT- and PTT-treated cells show an excessive presence of red cells in addition to green.

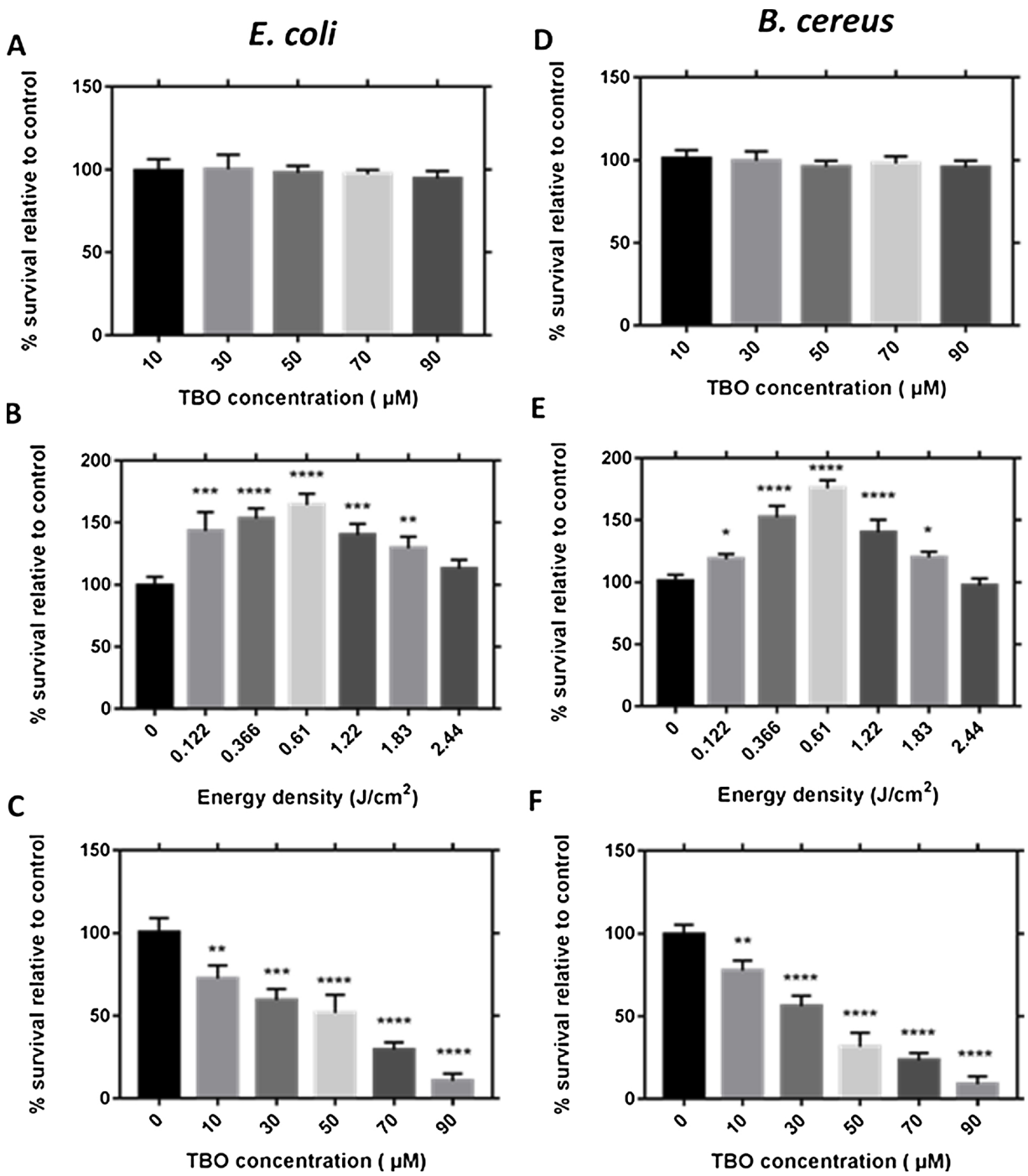

Fig. 4. Histograms show % survival relative to the control group (L-P-) for *B. cereus* and *E. coli* bacteria, for treated groups (A) L-P + , (B) L + P-, and (C) L + P + . Error bars represent standard error from three different experiments.

4. Discussion

Since TBO aggregation plays a critical role in its photodynamic process, this phenomenon was investigated by UV–vis absorption spectroscopy. The absorbance increased as the concentration increased and eventually split into two peaks, one with a maximum absorbance at 590 nm and the other with a maximum absorbance at 633 nm. The rising relative absorption of the peak at 590 nm with increasing TBO concentration clearly indicated the conversion of TBO monomers into dimer aggregates [35]. At a TBO concentration of 100 μM, the absorption at 590 nm becomes higher than that at 633 nm, which could be explained by Usacheva et al. [36] who stated that TBO dye changes its spectral behaviour due to electrostatic and hydrophobic interactions between the dye molecules as a result of aggregation. This behaviour, known as the metachromasy effect, manifests as a shift in the absorption maximum of a dye to a shorter wavelength (590 nm, hypochromic effect) and a decrease in its molar absorbance at the wavelength absorption maximum (633 nm, hypochromic effect). On the other hand, at a concentration of 1000 μM, the absorption band becomes very broad with a plateau shape, which indicates the presence of J- and H-type aggregates and the formation of higher aggregate species such as trimers, tetramers, and pentamers [34]. From the literature, the major spectroscopic effects due to dye aggregation mechanisms can be classified into three different types. The first effect is a hypsochromic shift

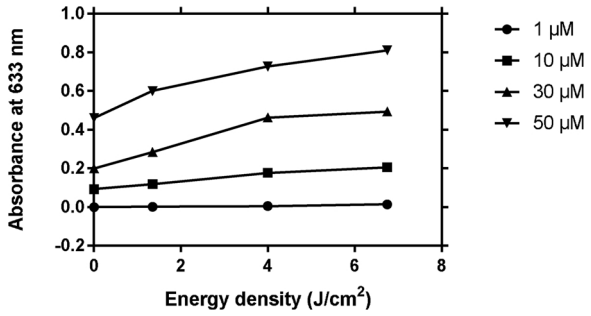

Fig. 5. The absorbance of TBO-bacterial suspension filtrates with different TBO concentrations after exposure to He-Ne laser for various irradiation times.

(blueshift) of the monomer absorption band towards the blue part of the spectrum, which results from what is called H-aggregation. In H-aggregation, the dye molecules arrange in parallel, forming a nearly vertical stack. The second effect is caused by J-aggregation, which causes a bathochromic shift (redshift) of the absorption band towards the red with respect to the monomer band. In this case, the dye molecules arrange head-to-tail, forming a slanting stack. In the third effect, band splitting (Davidov splitting) is observed, and both red and blue peaks appear; this effect is due to intermediate (oblique) aggregation [34].

Analogous to the UV–vis absorption study, the emission study revealed the effect of aggregation on the optical behaviour of the TBO molecules in aqueous solution. The fluorescence emission peak intensity increased with the concentration increase until the concentration reached 100 μM, at which point the fluorescence emission decreased due to the inner filter effect (IFE). The IFE can occur due to absorbing, excitation and/or emission of light by sample molecules that reduces the observed fluorescence intensity. The IFE results in a non-linear relationship between the observed fluorescence intensity and the concentration of the fluorescer [37,38].

Taking the results of the spectroscopic study of TBO into consideration, the concentrations used in the PDT treatment were restricted to the range of 10–90 μM to avoid high levels of aggregation.

Since its wavelength is compatible with the absorption maximum of TBO, a He-Ne laser was used as a source of irradiation in the PDT experiments. The effect of He-Ne laser light on *E. coli* and *B. cereus* was investigated in the absence of TBO (L + P-). The results showed that a low-power He-Ne laser has an enhancement effect on the survival of both bacterial strains. This proliferation effect reaches its maximum at 0.6 J/cm^2, where it showed a 165% increase in *E. coli* cell survival and a more than 176% increase in *B. cereus* cell survival. Although there are several articles about bacterial growth stimulation upon red light irradiation [39–41], the explanations of Tiina Karu [42] are still the most convenient. According to Karu, cytochrome *bd* and *bo* complexes are photoacceptors for red and near-IR radiation, which trigger mechanisms such as protein folding and shift the pH and overall redox state of cells in a more oxidized direction, while a secondary mechanism of action is proposed to cause a local increase in the temperature of the absorbing chromophores that could trigger biochemical activities such as activation or inhibition of enzymes. In particular, red and infrared light shifts the redox state of cells toward oxidation and enhances the synthesis of ATP and DNA. This can explain the photoinduced bacterial growth stimulation [43].

The PDT experiment results show that in the presence of a He-Ne laser, TBO exerts a significant inhibitory effect on the survival of each treated bacterium relative to that of the control. This is in agreement with a previous finding [12]. This inhibition increases with increasing concentrations of TBO for fixed doses of laser light. This effect reaches 90% of colonies with 90 μM TBO, which is very similar to previous results despite the very low laser dose compared to the laser dose in the previous literature [44].

Both G + ve and G-ve bacteria have an overall negatively charged cell surface composed of different surface structures. The anionic surface therefore acts as an electroattractive scaffold for the cationic TBO molecules. [26] However, at most concentrations, *B. cereus* was profoundly inhibited by the same concentration of TBO as *E. coli*. The different photodynamic responses of *E. coli* and *B. cereus* are due to their structural differences. It has been stated in the literature that in general, neutral or anionic PS molecules can efficiently bind and inactivate G + ve bacteria, whereas G-ve bacteria are relatively resistant to these compounds. Physiology explains the high susceptibility of G + ve bacteria, as their cytoplasmic membrane is surrounded by relatively porous layers of peptidoglycan and lipoteichoic acid, the latter of which contributes to the negative charge and provides binding sites for cationic molecules of TBO. In contrast, G-ve bacteria have a relatively thin cell wall peptidoglycan surrounded by a second lipid membrane containing lipopolysaccharide (LPSs) and lipoproteins [45].

Because TBO is a membrane-active dye with high affinity for acidic tissue components, it binds to the teichuronic acid (TA) residues of the outer wall, which are more commonly found in G + ve bacteria than in G-ve bacteria. This may explain why at most concentrations, *B. cereus* bacteria were more susceptible than *E. coli* to TBO. TBO predominantly binds to the LPS present in the G-ve outer cell envelope, which causes its PDT action on *E. coli*. [46,16] Moreover, the binding of the PS to LPSs competes with the binding of cations such as Ca^{2+} and Mg^{2+} that stabilize the bacterial membrane structure and integrity [26].

The PDT process could be summarized as follows: TBO molecules bind to the anionic components of the outer membrane, such as LPSs and TA, and then the divalent cation replacement in *E. coli* LPSs by cationic TBO leads to membrane distortion and pore formation to promote uptake, which is called self-promoted uptake [26]. Therefore, it is believed that the damage caused by PDT is irreversible.

In addition, the rapid increase in the absorbance of TBO-*E. coli* suspension filtrate at 633 nm after irradiation indicates an increase in TBO released into the surrounding medium. These results demonstrate the rapid membrane destruction caused by the PDT process and the release of TBO molecules that had been taken up by the cell. Furthermore, they supports the model of TBO molecules attaching to *E. coli* membranes and being released upon the destruction of those

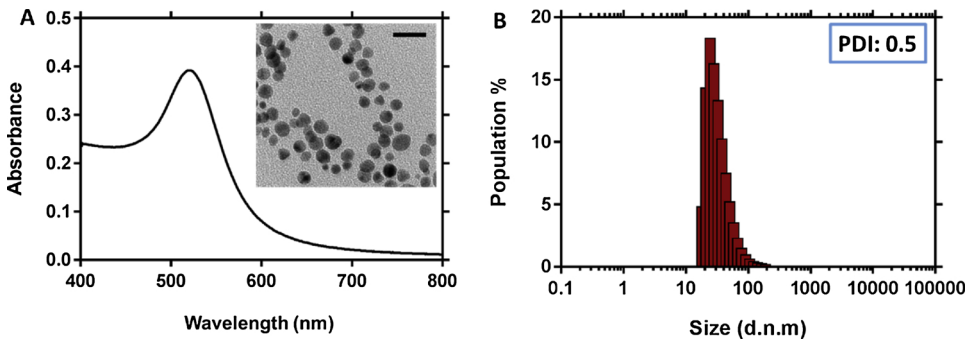

Fig. 6. Characterization of GNP-PVP A) UV–vis absorption spectrum shows a maximum absorption peak at 519 nm. Upper panel: TEM micrograph of GNP-PVP shows an average size of 15 ± 3 nm, and the scale bar is 20 nm. B) DLS histogram shows an average hydrodynamic diameter of 35 nm with a polydispersity index (PDI) of 0.5.

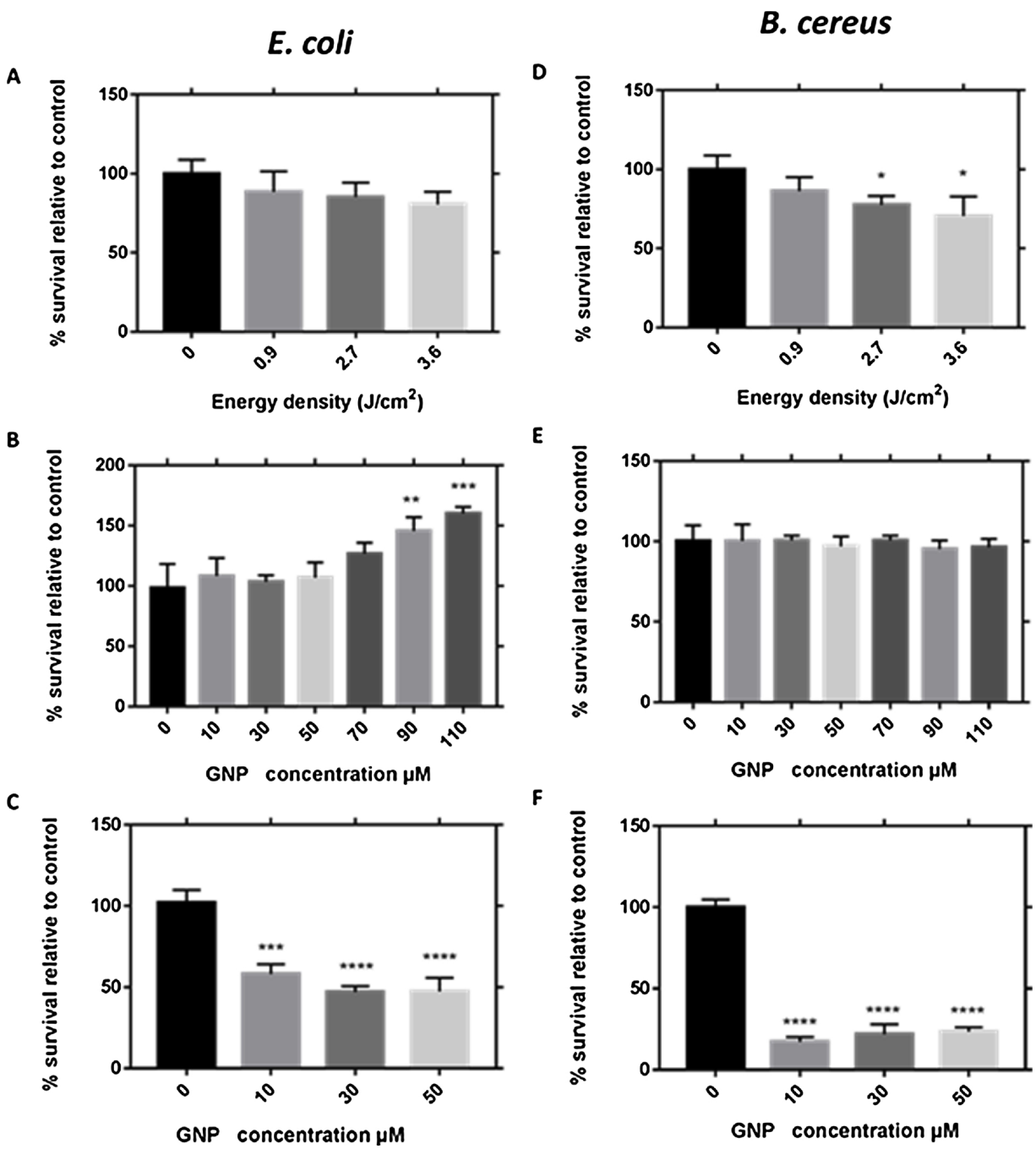

Fig. 7. % Survival relative to the control group (L-G-) of *B. cereus* and *E. coli* for treatment groups (A) L-G+, (B) L + G-, and (C) L + G+, the used GNP were capped with PVP. Error bars represent standard error from three different experiments.

membranes.

The PTT effect was studied in parallel with the PDT effect on *B. cereus* and *E. coli*. After GNP were prepared, the UV–vis absorption spectra of dilute aqueous solutions of GNP were recorded, and they showed an absorption maximum at 519 nm that confirmed the formation of particles approximately 20 nm in diameter. [47] This result was in agreement with the TEM micrograph that confirmed the formation of spherical particles with an average size of 15 ± 3 nm. The suspended GNP exhibited a hydrodynamic diameter of approximately 35 nm according to DLS. The hydrodynamic diameter obtained from the zetasizer was larger than the dry particle diameter obtained from the TEM imaging. This can be ascribed to the difference between the two techniques: while the outer PVP layer contributes to the DLS, it does not contribute to the TEM imaging [48,49]. The DLS analysis revealed the particle size distribution in the prepared sample and the PDI value, which was typically 0.5, ensuring homogeneity in particle size and shape [50].

Incubation of *E. coli* and *B. cereus* cells with GNP-PVA in the dark resulted in fewer surviving bacteria in these groups than in the control groups (Fig. 2S), which could be due to the presence of PVA on the surface of the GNP. Although PVA is a biodegradable synthetic polymer that is not carcinogenic, it also has antimicrobial activity. This finding is in accordance with results reported in previous studies, *e.g.*, Lyoo et al [51] reported that the enhanced antimicrobial properties of PVA could be an important advantage in biomedical applications. Additionally, Tunku Kamarul et al [52] demonstrated that PVA implantation induced some acute tissue responses *in vivo*.

In contrast, the two bacterial strains showed different growth

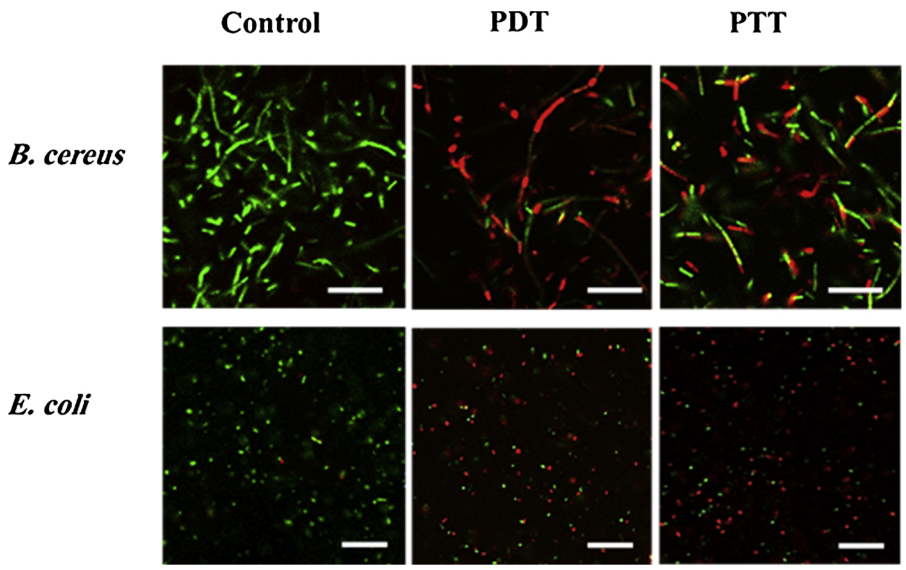

Fig. 8. Live/dead imaging of *E. coli* and *B. cereus* cells showing the control, PDT (L + P+), and PTT (L + G+) groups. Acridine orange stained cells represent the live cells (green), while the PI-stained cells represent the dead cells (red). Scale bars equal to 20 μm.

behaviour when incubated with GNP-PVP in dark conditions (L-G+). *E. coli* showed similar growth to the control group (L-G-) at GNP-PVP concentrations up to 50 μM, while increasing GNP-PVP concentrations from 50 to 110 μM increased the cell growth above that of the control. On the other hand, *B. cereus* cells incubated with GNP-PVP in the dark showed normal growth relative to that of the control group at all GNP-PVP concentrations.

These results are in agreement with the findings of Amin et al [53], who applied GNP-PVP to bacteria, and Villiers et al [54] and Min Zhou et al [55], who applied GNP-PVP to human cells. After 24 h post-treatment, the cells showed excellent viability at GNP-PVP concentrations even up to 100 μM. These results may be explained by PVP possibly providing a non-toxic coating to **gold** nanoparticles. The growth increase observed for *E. coli* may be due to the catalytic activity of trace amounts of PVP. [56] On the basis of the above results, the PTT experiments in this study used 10, 30 and 50 μM GNP-PVP, since these concentrations have a mild effect on bacterial growth in the dark.

As its wavelength was within the SPR peak of the GNP, an LED producing 532 nm light was used. The effect of green LED alone (L + G-) on E. coli and B. cereus cells was studied to determine a safe laser dose for both bacterial strains. Irradiation with the LED at doses up to 3.6 J/cm^2 did not significantly inhibit E. coli cell growth. This result agrees with the results of Yana Reznick et al., who exposed the gram-negative bacteria *Pseudomonas aeruginosa* to green laser light at a wavelength of 532 nm. [57] However, green light reduced the growth of B. cereus to 90%, 72% and 55% that of the control as the irradiation dose was increased to 0.9, 2.7 and 3.6 J/cm^2, respectively. This could be due to the stimulation of certain porphyrins and/or flavoproteins normally located inside the cells, since porphyrin has an absorption band at 540 nm. The variation in the distribution and amounts of porphyrins in *E. coli* and *B. cereus* could cause the difference in the photoresponses of these organisms. [58] These results corroborate that the G + ve bacteria are more susceptible to inactivation by visible light than G-ve bacteria [59].

The PTT experiment was designed based on the results of the experiments studying the influence of each factor on the PTT process independently. Three concentrations of GNP (10, 30 and 50 μM) were applied with 0.9 J/cm^2 intensity from the LED.

A significant reduction in bacterial survival was observed in photothermally treated bacteria relative to the control bacteria. GNP in combination with the LED gave 40% *E. coli* survival inhibition relative to the survival of the control group and 75% *B. cereus* survival inhibition relative to the survival of the control group. This result resembles the results of Safan et al. [60]

The observed antibacterial activity is due to the hyperthermia induced in the medium upon irradiation of GNP with the appropriate light. As a result, GNP generate heat in their surroundings, which causes irreversible cell damage by permeabilizing cell membranes and denaturing proteins and a reduction in bacterial growth. [61]

On the other hand, the photothermal responses of *E. coli* and *B. cereus* differ due to the structural differences between these two species. The difference between the outer walls of G + ve and G-ve is in the degree of permeability. The outer wall of G-ve bacteria acts as a barrier due to the presence of an LPS layer that can exclude macromolecules and hydrophilic substances, resulting in the intrinsic resistance of G-ve bacteria to the gold nanoparticles. Therefore, *B. cereus* is more susceptible to the photothermal effect of GNP than *E. coli*. [45]

E. coli and *B. cereus* bacteria were stained with an AO/PI mixture and visualized under a CLSM to study the membrane integrity of each strain after PDT and PTT treatments. While the AO stain can be internalized into live cells, the PI stain can enter only damaged cells. From the CLSM imaging, we can see the control groups from both strains showing almost exclusively green cells, indicating the presence of AO-stained cells only. Meanwhile, PDT- and PTT-treated cells show an excessive presence of red cells in addition to green cells. This indicates the presence of many dead cells with damaged membranes that internalized PI, resulting in the red fluorescence. [33]

5. Conclusions

The exponential increase in MDR bacteria has highlighted the high demand for new alternative treatments for localized infections. PDT and PTT are new techniques that may be used as innovative antimicrobial remedies. In this study, both PDT and PTT were applied in very carefully chosen conditions, allowing us to study the real effect of PDT/PTT separate from the individual effects of the elements contributing to the PDT/PTT techniques. Herein, it is apparent that PDT using TBO is an excellent antibacterial therapy because it requires lasers whose wavelengths are within the window of 600–900 nm, which are more suitable for the treatment of human conditions than other wavelengths. Moreover, from this study, it is apparent that PTT using GNP gives us new prospects for fighting MDR bacteria. Both G-ve and G + ve bacteria were inhibited by PDT/PTT, although the species showed slightly different survival percentages, which may result from the peculiar structural differences between G-ve and G + ve bacterial

membranes. Ultimately, we can conclude that PDT and PTT are particularly useful in the phototherapy of both G-ve and G + ve bacteria. To make PDT/PTT more practical for clinical use, higher doses of PSs/nanoparticles and laser light can be used to achieve complete bacterial eradication and reduce the photoexposure period. In future work, the bacterial eradication advantage can be enhanced by using combinations of PTT and PDT.

Declaration of Competing Interest

The authors declare no conflict of interest.

Aknowlagement

The authors are indebted to Prof. Jehan Al Moghazy (Food Safety and Biotechnology Laboratory, Regional Center for Food and Feed, Agriculture Research Center, Egypt) for providing the bacterial strains, and Dr. Emily Crawford (Chan Zuckerberg Biohub,SF, USA) for her help in revising the manuscript.

Appendix A. Supplementary data

Supplementary material related to this article can be found, in the online version, at doi:https://doi.org/10.1016/j.pdpdt.2019.06.020.

References

[1] L. Lucijanovic, A. Dukic, The global threat of antimicrobial resistance: science for intervention, Nase More 47 (1–2) (2015) 53–55, https://doi.org/10.1016/j.nmni.2015.02.007.
[2] O.M. Ibrahim, M. Saber-ayad, Antibiotic misuse in different hospital wards (a pilot study in an egyptian academic sciences asian journal of pharmaceutical and clinical research, No. May 2014 (2012) 1–4.
[3] N.A. Sabry, S.F. Farid, D.M. Dawoud, Antibiotic dispensing in egyptian community pharmacies: an observational study, Res. Social Adm. Pharm. 10 (1) (2014) 168–184, https://doi.org/10.1016/j.sapharm.2013.03.004.
[4] M. Zakaa El-din, F. Samy, A. Mohamed, F. Hamdy, S. Yasser, M. Ehab, Egyptian community pharmacists' attitudes and practices towards antibiotic dispensing and antibiotic resistance; a cross-sectional survey in Greater Cairo, Curr. Med. Res. Opin. 0 (0) (2018) 1–8, https://doi.org/10.1080/03007995.2018.1544119.
[5] A.M. Ammar, E.E. Abdeen, U.H. Abo-Shama, E. Fekry, E. Kotb Elmahallawy, Molecular characterization of virulence and antibiotic resistance genes among *Salmonella* serovars isolated from broilers in Egypt, Lett. Appl. Microbiol. (2019), https://doi.org/10.1111/lam.13106.
[6] U. Theuretzbacher, Global antibacterial resistance: the never-ending story, J. Glob. Antimicrob. Resist. 1 (2) (2013) 63–69, https://doi.org/10.1016/j.jgar.2013.03.010.
[7] M. Wainwright, Tricyclic cationic chromophores as models for new photoantimicrobials, J. Braz. Chem. Soc. 26 (12) (2015) 2390–2404, https://doi.org/10.5935/0103-5053.20150188.
[8] D. Dave, U. Desai, N. Despande, Photodynamic therapy : a view through light, J. Orofac. Res. 2 (2) (2012) 82–86.
[9] Thomas J. Dougherty, Charles J. Gomer, Barbara W. Henderson, et al., Photodynamic therapy, J. Natl. Cancer Inst. 90 (12) (1998) 889–905, https://doi.org/10.1016/j.ygyno.2014.12.035.Pharmacologic.
[10] M. Miyabe, J.C. Junqueira, A.C.B.P. da Costa, A.O.C. Jorge, M.S. Ribeiro, I.S. Feist, Effect of photodynamic therapy on clinical isolates of Staphylococcus spp, Braz. Oral Res. 25 (3) (2011) 230–234, https://doi.org/10.1590/S1806-83242011005000006.
[11] L.M. Moreira, J.P. Lyon, A.P. Romani, D. Severino, M.R. Rodrigues, H.P.M. de Oliveira, Phenotiazinium dyes as photosensitizers (PS) in photodynamic therapy (PDT): spectroscopic properties and photochemical mechanisms, In Adv. Asp. Spectr. (2012) 393–422, https://doi.org/10.5772/48087.
[12] H.K. Nielsen, J. Garcia, M. Væth, S. Schlafer, Comparison of Riboflavin and toluidine blue O as photosensitizers for photoactivated disinfection on endodontic and periodontal pathogens in vitro, PLoS One 10 (10) (2015) 1–11, https://doi.org/10.1371/journal.pone.0140720.
[13] K. Biberoglu, M.Y. Tek, S.T. Ghasemi, O. Tacal, Toluidine blue O is a potent inhibitor of human cholinesterases, Arch. Biochem. Biophys. 604 (2016) 57–62, https://doi.org/10.1016/j.abb.2016.06.005.
[14] A. Delport, B.H. Harvey, A. Petzer, J.P. Petzer, The monoamine oxidase inhibition properties of selected structural analogues of methylene blue, Toxicol. Appl. Pharmacol. 325 (2017) 1–8, https://doi.org/10.1016/j.taap.2017.03.026.
[15] D. Atiakshin, V. Samoilova, I. Buchwalow, W. Boecker, M. Tiemann, Characterization of mast cell populations using different methods for their identification, Histochem. Cell Biol. 147 (6) (2017) 683–694, https://doi.org/10.1007/s00418-017-1547-7.
[16] G. Sridharan, Aa. Shankar, Toluidine blue: a review of its chemistry and clinical utility, J. Oral Maxillofac. Pathol. 16 (2) (2012) 251–255, https://doi.org/10.4103/0973-029X.99081.
[17] J.C. da Silva Passos, M. Lopes Carvalho, F. Villaça Morais, M. Silva Costa, Photodynamic Antimicrobial Chemotherapy (PACT), Using Toluidine Blue (TBO) Inhibits Both Growth and Dimorphism in Paracoccidioides Brasiliensis by a Mechanism Involving Reactive Oxygen Species (ROS) Production, Photodiagnosis Photodyn. Ther. (2019), https://doi.org/10.1016/J.PDPDT.2019.01.003.
[18] M. Wainwright, C. O'Kane, S. Rawthore, Phenothiazinium photosensitisers XI. Improved toluidine blue photoantimicrobials, J. Photochem. Photobiol. B, Biol. 160 (2016) 68–71, https://doi.org/10.1016/j.jphotobiol.2016.03.035.
[19] M. Aioub, L.A. Austin, M.A. El-Sayed, Gold nanoparticles for cancer diagnostics, spectroscopic imaging, drug delivery, and plasmonic photothermal therapy, Chapter 2, in: A. M. B. T.-I. F. as S. N (Ed.), *Inorganic Frameworks as Smart Nanomedicines*; Grumezescu, William Andrew Publishing, 2018, pp. 41–91, , https://doi.org/10.1016/B978-0-12-813661-4.00002-X.
[20] Qiongchan Gu, Hang Zhao, Bowen Xu, Xiaoxiao Jiang, J. Lv, Photothermal modeling of plasmonic nanostructures: a review, Nanosci. Nanotechnol. Lett. 9 (5) (2017) 599–608.
[21] D. Pissuwan, S.M. Valenzuela, M.B. Cortie, Therapeutic possibilities of plasmonically heated gold nanoparticles, Trends Biotechnol. 24 (2) (2006) 62–67, https://doi.org/10.1016/j.tibtech.2005.12.004.
[22] X. Huang, P.K. Jain, I.H. El-Sayed, M.A. El-Sayed, Plasmonic photothermal therapy (PPTT) using gold nanoparticles, Lasers Med. Sci. 23 (3) (2008) 217–228, https://doi.org/10.1007/s10103-007-0470-x.
[23] J.W. Stone, A.M. Alkilany, M.A. Hamaly, S. Canonico-May, Biomedical applications of anisotropic Gold nanoparticles, in: S.E. Hunyadi Murph, G.K. Larsen, K.J. Coopersmith (Eds.), *Anisotropic and Shape-Selective Nanomaterials: Structure-Property Relationships*, Springer International Publishing: Cham, 2017, pp. 399–426, , https://doi.org/10.1007/978-3-319-59662-4_13.
[24] N. Elahi, M. Kamali, M.H. Baghersad, Recent biomedical applications of gold nanoparticles: a review, Talanta 184 (2018) 537–556, https://doi.org/10.1016/j.talanta.2018.02.088.
[25] T.H. Michael Hamblin, Photodynamic Therapy: A New Antimicrobial Approach to Infectious Disease, Photochem. Photobiol. 3 (5) (2011) 436–450, https://doi.org/10.1039/b311900a.Photodynamic.
[26] Y. Liu, R. Qin, S.A.J. Zaat, E. Breukink, M. Heger, Antibacterial photodynamic therapy: overview of a promising approach to fight antibiotic-resistant bacterial infections, J. Clin. Transl. Res. 1 (3) (2015) 140–167, https://doi.org/10.18053/jctres.201503.002.
[27] F. Barra, E. Roscetto, A.A. Soriano, A. Vollaro, I. Postiglione, G.M. Pierantoni, G. Palumbo, M.R. Catania, Photodynamic and antibiotic therapy in combination to fight biofilms and resistant surface bacterial infections, Int. J. Mol. Sci. 16 (9) (2015) 20417–20430, https://doi.org/10.3390/ijms160920417.
[28] M. Wainwright, A. McLean, Rational design of phenothiazinium derivatives and photoantimicrobial drug discovery, Dyes Pigm. 136 (2017) 590–600, https://doi.org/10.1016/j.dyepig.2016.09.015 2017.
[29] J. Odeberg, A. Wirsén, Å. Norberg, J. Frie, G. Printz, H. Lagercrantz, G.H. Gudmundsson, B. Agerberth, B. Jonsson, A novel cysteine-linked antibacterial surface coating significantly inhibits bacterial colonization of nasal silicone prongs in a phase one pre-clinical trial, Mater. Sci. Eng. C 93 (October 2017) (2018) 782–789, https://doi.org/10.1016/j.msec.2018.08.040.
[30] K. Komagoe, H. Kato, T. Inoue, T. Katsu, Continuous real-time monitoring of cationic porphyrin-induced photodynamic inactivation of bacterial membrane functions using electrochemical sensors, Photochem. Photobiol. Sci. 10 (7) (2011) 1181–1188, https://doi.org/10.1039/c0pp00376j.
[31] K. Dong, J. Zhou, T. Yang, S. Dai, H. Tan, Y. Chen, H. Pan, J. Chen, B. Audit, S. Zhang, et al., Sensitive Hg2 + ion detection using metal enhanced fluorescence of novel polyvinyl pyrrolidone (PVP)-Templated gold nanoparticles, Appl. Spectrosc. 72 (11) (2018) 1645–1652, https://doi.org/10.1177/0003702818775704.
[32] I. Tokareva, E. Hutter, Hybridization of oligonucleotide-modified silver and gold nanoparticles in aqueous dispersions and on gold films, J. Am. Chem. Soc. 126 (48) (2004) 15784–15789, https://doi.org/10.1021/ja046779k.
[33] S.B. Subramaniyan, A. Ramani, V. Ganapathy, V. Anbazhagan, Preparation of self-assembled platinum nanoclusters to combat Salmonella typhi infection and inhibit biofilm formation, Colloids Surf. B Biointerfaces 171 (2018) 75–84, https://doi.org/10.1016/j.colsurfb.2018.07.023.
[34] L. D'Ilario, A. Martinelli, Toluidine blue: aggregation properties and structural aspects, Model. Simul. Mater. Sci. Eng. 14 (2006) 581, https://doi.org/10.1088/0965-0393/14/4/003.
[35] S. Dasmandal, D. Bhattacharyya, S. Rudra, B.K. Patel, A. Mahapatra, Spectroscopic Investigation on Interaction of Toluidine Blue/ AOT/ γ-Cyclodextrin Ternary System, J. Lumin. 179 (2016) 340–349, https://doi.org/10.1016/j.jlumin.2016.06.057 2016.
[36] M.N. Usacheva, M.C. Teichert, M.A. Biel, The role of the methylene blue and toluidine blue monomers and dimers in the photoinactivation of Bacteria, J. Photochem. Photobiol. B, Biol. 71 (1–3) (2003) 87–98, https://doi.org/10.1016/j.jphotobiol.2003.06.002.
[37] S. Chen, Y.-L. Yu, J.-H. Wang, Inner filter effect-based fluorescent sensing systems: a review, Anal. Chim. Acta 999 (2018) 13–26, https://doi.org/10.1016/j.aca.2017.10.026.
[38] M. Yang, Y. Yan, H. Shi, C. Wang, E. Liu, X. Hu, J. Fan, Efficient inner filter effect sensors based on CdTeS quantum dots and Ag nanoparticles for sensitive detection of L-Cysteine, J. Alloys. Compd. 781 (2019) 1021–1027, https://doi.org/10.1016/j.jallcom.2018.12.156.
[39] R.N. Khramov, A.P. Glinushkin, E.V. Barmina, N.F. Bunkin, S.N. Andreev,

B.B. Kartabaeva, N.I. Taranda, E.V. Stepanov, S.V. Gudkov, A.P. Nesvat, Effect of visible light on biological objects: physiological and pathophysiological aspects, Phys. Wave Phenom. 25 (3) (2017) 207–213, https://doi.org/10.3103/s1541308x17030074.

[40] A.M. Ali, The effect of 650 nm diode laser on growth curve of gram-negative Bacteria and their phagocytic killing assay by PMN cells, Iraqi J. Sci. 56 (3B) (2015) 2264–2274.

[41] J. Tafur, P.J. Mills, Low-intensity light therapy: exploring the role of redox mechanisms, Photomed. Laser Surg. 26 (4) (2008) 323–328, https://doi.org/10.1089/pho.2007.2184.

[42] T.I., K, Primary and secondary mechanisms of action of visible to near-IR radiation on cells, J. Photochem. Photobiol. B, Biol. 49 (1) (1999) 1–17, https://doi.org/10.1016/S1011-1344(98)00219-X.

[43] M.V. Trushin, The effect of red and infrared light on the growth of Escherichia coli and the production of the recombinant protein barstar, Microbiology 71 (4) (2002) 383–385, https://doi.org/10.1023/A:1019877023168.

[44] H. Mahmoudi, A. Bahador, M. Pourhajibagher, M.Y. Alikhani, Antimicrobial photodynamic therapy: an effective alternative approach to control bacterial infections, J. Lasers Med. Sci. 9 (3) (2018) 154–160, https://doi.org/10.15171/jlms.2018.29.

[45] P.C. Liaw, B.L. Trigatti, N.G. Seidah, D.J. Dwivedi, A. Prat, P.M. Grin, K.M. Chathely, A.E. Fox-Robichaud, Low-density lipoprotein (LDL)-Dependent uptake of gram-positive lipoteichoic acid and gram-negative lipopolysaccharide occurs through LDL receptor, Sci. Rep. 8 (1) (2018) 1–11, https://doi.org/10.1038/s41598-018-28777-0.

[46] R. Fekrazad, H. Zare, S.M.S. Vand, Photodynamic therapy effect on cell growth inhibition induced by Radachlorin and toluidine blue O on Staphylococcus aureus and Escherichia coli: an in vitro study, Photodiagnosis Photodyn. Ther. 15 (2016) 213–217, https://doi.org/10.1016/j.pdpdt.2016.07.001 2016.

[47] S. Link, M.A. El-Sayed, Size and temperature dependence of the plasmon absorption of colloidal gold nanoparticles, J. Phys. Chem. B 103 (21) (1999) 4212–4217, https://doi.org/10.1021/jp984796o.

[48] T. Zheng, S. Bott, Q. Huo, Techniques for accurate sizing of gold nanoparticles using dynamic light scattering with particular application to chemical and biological sensing based on aggregate formation, ACS Appl. Mater. Interfaces 8 (33) (2016) 21585–21594, https://doi.org/10.1021/acsami.6b06903.

[49] L. Shang, R.M. Dörlich, S. Brandholt, R. Schneider, V. Trouillet, M. Bruns, D. Gerthsen, G.U. Nienhaus, C. Joo, H. Balci, et al., Facile preparation of water-soluble fluorescent gold nanoclusters for cellular imaging applications, Nanoscale 3 (5) (2011) 2009, https://doi.org/10.1039/c0nr00947d.

[50] S.D.L.S. Bhattacharjee, Zeta Potential, What they are and what they are not? J. Control. Release 235 (2016) 337–351, https://doi.org/10.1016/j.jconrel.2016.06.017.

[51] W.S. Lyoo, S.S. Han, W.S. Yoon, B.C. Ji, J. Lee, Y.W. Cho, J.H. Choi, W.S. Ha, Syndiotacticity-rich ultrahigh molecular-weight poly(vinyl alcohol) film. I. Determination of optimum polymer concentration by zone-drawing method in film preparation, J. Appl. Polym. Sci. 77 (1) (2000) 123–134, https://doi.org/10.1002/(SICI)1097-4628(20000705)77:1<123::AID-APP17>3.0.CO;2-J.

[52] Tunku Kamarul, G. Krishnamurithy, Noman D. Salih, Nurul Syuhada Ibrahim, Hanumantha Rao Balaji Raghavendran, Abdul Razzaq Suhaeb, D. S. K. C, Biocompatibility and toxicity of poly(vinyl alcohol)/N,O-Carboxymethyl chitosan scaffold, Transfus. Apher. Sci. (2014) 1–7 2014.

[53] R.M. Amin, M.B. Mohamed, M.A. Ramadan, T. Verwanger, B. Krammer, Rapid and sensitive microplate assay for screening the effect of silver and gold nanoparticles on Bacteria, Nanomedicine 4 (6) (2009) 637–643, https://doi.org/10.2217/nnm.09.50.

[54] A.M. Alkilany, C.J. Murphy, Toxicity and cellular uptake of gold nanoparticles: what we have learned so far? J. Nanopart. Res. 12 (7) (2010) 2313–2333, https://doi.org/10.1007/s11051-010-9911-8.

[55] M. Zhou, B. Wang, Z. Rozynek, Z. Xie, J.O. Fossum, X. Yu, S. Raaen, Minute synthesis of extremely stable gold nanoparticles, Nanotechnology 20 (50) (2009) 505606, , https://doi.org/10.1088/0957-4484/20/50/505606.

[56] R. Rashid, N.S.J. Lim, S.M.L. Chee, S.N. Png, T. Wohland, M. Raghunath, Novel use for polyvinylpyrrolidone as a macromolecular crowder for enhanced extracellular matrix deposition and cell proliferation, Tissue Eng. Part C Methods 20 (12) (2014) 994–1002, https://doi.org/10.1089/ten.TEC.2013.0733.

[57] Y. Reznick, E. Banin, A. Lipovsky, R. Lubart, Z. Zalevsky, Direct laser light enhancement of susceptibility of Bacteria to gentamicin antibiotic, Opt. Commun. 284 (23) (2011) 5501–5507, https://doi.org/10.1016/j.optcom.2011.08.025.

[58] S. Dadras, E. Mohajerani, F. Eftekhar, M. Hosseini, Different photoresponses of Staphylococcus aureus and Pseudomonas aeruginosa to 514, 532, and 633 nm low level lasers in vitro, Curr. Microbiol. 53 (4) (2006) 282–286, https://doi.org/10.1007/s00284-005-0490-3.

[59] M.C. Decarli, M.T. Carvalho, T.Q. Corrêa, et al., Different Photoresponses of Microorganisms : From Bioinhibition to Biostimulation, Curr. Microbiol. 72 (4) (2016) 473–481, https://doi.org/10.1007/s00284-015-0976-6.

[60] I. Journal, O.F. Advanced, M. Zaazou, S.I. Abd, Antibacterial effect of silver & gold nanoparticles and diode laser against Lactobacillus acidophilus Bacteria, Int. J. Adv. Res. (Indore) 2 (8) (2014) 34–38.

[61] A. Bucharskaya, G. Maslyakova, G. Terentyuk, A. Yakunin, Y. Avetisyan, O. Bibikova, E. Tuchina, B. Khlebtsov, N. Khlebtsov, Towards effective photothermal/photodynamic treatment using plasmonic gold nanoparticles, Int. J. Mol. Sci. 17 (1295) (2016) 1–26, https://doi.org/10.3390/ijms17081295.